2004-01-1528

DEEP ROLLING RESPONSE OF NOTCHED MEDIUM CARBON BAR STEELS

Mark D. Richards, David K. Matlock, and John G. Speer
Advanced Steel Processing and Products Research Center, Colorado School of Mines

ABSTRACT

The effects of deep rolling were evaluated by reviewing the fatigue performance of three medium-carbon (0.4 C) bar steels representing microstructural classes characteristic of forging steels used for crankshaft and other automotive applications. Deep rolling is a surface deformation process whereby a radially symmetric work piece undergoes a surface deformation operation. The steel grades included a quenched and tempered alloy steel (4140) that demonstrated a high yield stress and low strain hardening rate, a non-traditional bainitic experimental grade (1.2 Mn, 0.72 Si) containing high amounts of retained austenite with low yield stress and high strain hardening rate, and a ferritic/pearlitic grade (1.3 Mn, 0.56 Si) with a low yield stress and medium strain rate hardening rate.

A reproducible test methodology to assess fatigue behavior was developed, based on flex-beam, fully reversed, S-N type laboratory fatigue testing. The as-received fatigue behavior of the three steels was characterized to provide a basis for comparison with the deep rolled condition. The deep rolling process was optimized in terms of rolling load based on peak fatigue life at an imposed nominal stress level for each steel. These conditions were used to process fatigue specimens for the final deep rolled condition. From the deep rolled specimens, the hardness profile and fatigue behavior were characterized. The fatigue data, fracture characteristics, and hardness profile data, are interpreted based on the consideration of the microstructure and corresponding strain hardening behavior as measured in compression and tensile tests.

INTRODUCTION

Surface-modification processes are used extensively to improve the fatigue performance of highly stressed components. Common processes based on heat treating include surface hardening, carburizing, and carbonitriding. Other methods derive improvements in fatigue performance from cold working and non-uniform plastic strains resulting from processes such as shot peening and deep rolling. Deep rolling, the subject of this paper, is a fatigue-performance-driven, surface modification process whereby roller tooling is applied to a radially symmetric component to plastically deform the near-surface layers. Deep rolling is primarily used to control surface hardness, surface finish, radial profile, and the residual stress characteristics in finished parts (1). The variables influencing the deep rolling process are the workpiece and roller geometries, the applied rolling load, and the number of over-rollings (number of rolling passes).

Crankshafts, axle shafts, and fasteners have been the primary areas of interest for the application of deep rolling. Cast iron crankshafts were the primary subject of initial deep rolling research (1-3). In these cases cast iron crankshafts were deep rolled and tested in a flex beam type test. Other studies with cast iron were performed on smaller, rotating bending type fatigue specimens (4,5). These results have been used over the years as a means to empirically control the deep rolling process for cast iron and wrought steel products. Fewer studies have investigated the effects of deep rolling on steels; these have primarily focused on ultimate tensile strengths and their relationship to the deep rolled fatigue strength (6,7).

Process control for deep rolling has employed an equation relating roller contact stress and applied load. Based upon ductile cast iron data it has been empirically determined that the contact stress should be 3-5 times the UTS of the workpiece material (1-3). The associated rolling force may be estimated from Equation [1], which shows the Hertzian contact stress for contacting cylinders or spheres of similar elastic modulus (2).

$$G = \sqrt{(0.175)\times\left(\frac{F\times E}{B}\right)\times\left(\frac{1}{\frac{D_1}{2}}+\frac{1}{\frac{D_2}{2}}\right)} \qquad [1]$$

Where:
- G = Specific Area Pressure (psi)
- F = Rolling Force (lbs.)
- E = Modulus of Elasticity (psi)
- B = Contact Length (in.)
- D_1 = Diameter of Work Roller (in.)
- D_2 = Diameter of Workpiece (in.)

Of the parameters influencing the deep rolling process (rolling load, geometry, and over-rollings), assessments of the effects of rolling load and geometry have been the primary focus of previous deep rolling research. With an increase in rolling load, the fatigue properties were found to improve until a maximum was achieved. A further increase in the applied load was detrimental to fatigue performance (4-7). This point is illustrated in Figure 1 that shows the effects of rolling load on the rotating bending fatigue strength of a 0.4 C, 0.8 Mn, 1.1 Cr steel (German steel grade 37 CrS 4) tempered to produce ultimate tensile strengths between 1150 and 1650 MPa and processed with 45 over-rollings. Also shown is one set of data for the 1150 MPa condition processed using 15 over-rollings (6). The fatigue strength achieved at the peak performance deep rolling condition depends significantly on the tensile strength of the material and to a lesser extent on the number of over-rollings (6). The optimized response can also vary greatly with differences in specimen notch geometries, characterized by stress concentration values, as shown in Figure 2 (7). Figure 2 shows the combined effects of stress concentration (k_t=1 to k_t=3) in 6.9 mm diameter (at root of notch) cylindrical samples and the roller geometries on the fatigue response of the 1150 MPa steel considered in Figure 1. For the smooth sample (k_t=1) the rolling load has only a slight improvement on fatigue performance. In contrast for samples with a notch (k_t=2 and k_t=3) an increase in rolling load significantly increases fatigue resistance, an observation attributed to higher residual compressive stresses induced because of the lateral constraints imposed by the sides of the notch on the localized plastic flow in the root of the notch upon rolling (4-7).

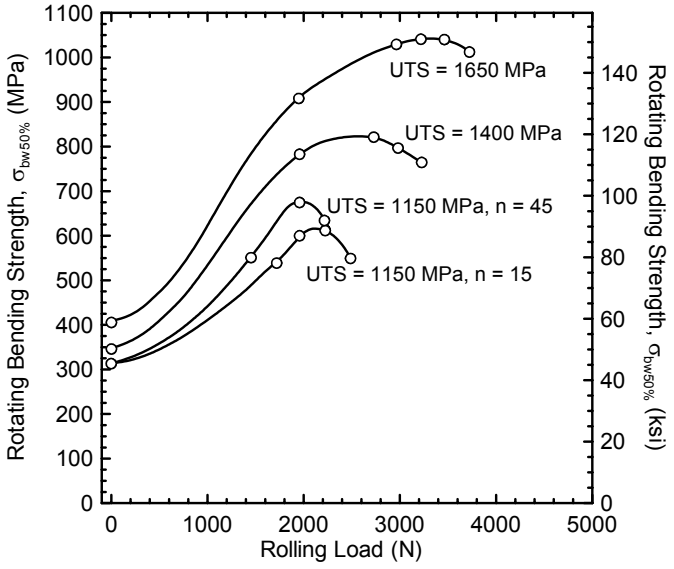

Figure 1. Rotating bending fatigue strength versus rolling load for German steel grade 37 CrS 4 quenched and tempered to the indicated strength levels (specimen diameter 6.9 mm, k_t=2, n is number of over-rollings) (re-plotted from (6)).

Previous deep rolling studies on cast iron and wrought steel have primarily correlated rolling response to a single mechanical property measured for the material of interest, i.e. the ultimate tensile strength. In this study the interrelationships between process dependent microstructure, microstructurally dependent strain-hardening behavior, and the strain-hardening dependent response of plastic deformation to deep rolling, are investigated with respect to the rolling pressure, as assessed through fatigue. This study considers the importance of incorporating the strain hardening behavior into deep rolling design criteria and incorporates a simplified laboratory scale fatigue test specimen and methodology.

MATERIALS

Three medium carbon bar steels with microstructures characteristic of forging steels of interest for crankshaft and other automotive applications, were evaluated. The three steels were selected based upon alloy content, processing histories, and anticipated strain-hardening behavior. These included a quenched and tempered (4140) steel, containing Mo and Cr, a non-traditional bainitic (NTB) steel alloyed with Mo, V, Ti, and Si, and an as hot-rolled ferritic/pearlitic low alloy (C38M) steel, alloyed with Mn, S, and Si. The chemical compositions of the three steels are listed in Table 1.

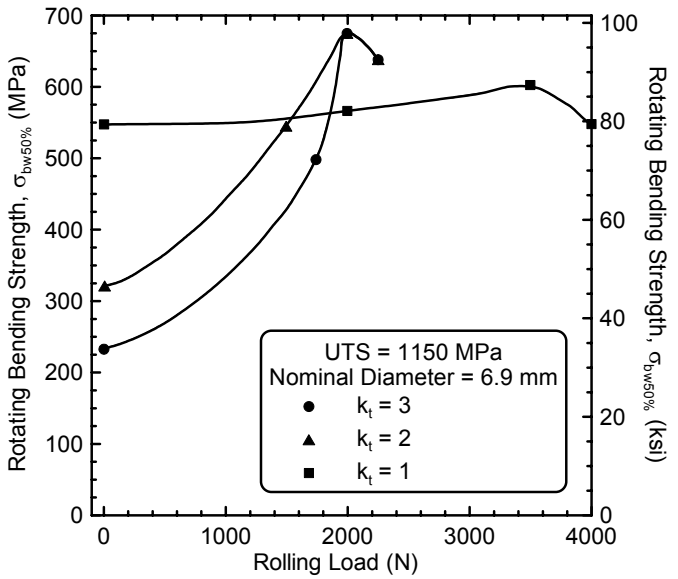

Figure 2. Rotating bending stress versus rolling load for the quenched and tempered steel from Figure 1 with a UTS of 1150 MPa. Optimization curves are shown for 6.9 mm diameter smooth sample (stress concentration factor , k_t, of 1) and 6.9 mm diameter notched sample with stress concentration factors of 2 and 3 (re-plotted from (7)).

Table 1. Chemical Compositions of Steels (wt. %)

Steel	C	Mn	S	Si	Ni
4140	0.45	0.85	0.041	0.20	0.10
NTB	0.38	1.21	0.011	0.73	0.12
C38M	0.41	1.30	0.067	0.56	0.09
Steel	**Cr**	**Mo**	**V**	**Al**	**Ti**
4140	0.85	0.22	0.005	0.026	0.002
NTB	0.09	0.22	0.099	0.014	0.023
C38M	0.11	0.03	0.011	0.036	0.005

The 4140 alloy was received as 32 mm diameter, quenched and tempered bars at a hardness of 30 HRC. The tempered martensitic microstructure is shown in Figure 3, a scanning electron micrograph of a sample etched in 2% nital. The 4140 alloy steel is a widely used forging and heat treating steel with applications from crankshafts to axle shafts. The NTB steel was received as 28.5 mm diameter, hot-rolled and direct cooled bars at a hardness of 25 HRC. The microstructure, as shown in the SEM micrograph in Figure 4, is primarily a modified bainitic microstructure in which some of the traditional bainitic carbides are replaced with retained austenite or martensite plus retained austenite (MA) constituents. Based on X-ray diffraction analysis the NTB steel contained 14.5 percent retained austenite with 1.63 weight percent carbon in the austenite. The C38M was received as 127 mm diameter, hot-rolled bars at a hardness of 25 HRC. The microstructure, shown in the SEM micrograph in Figure 5, consists of ferrite and pearlite. Also present are MnS particles, a consequence of higher sulfur content, which results in improved machinability. C38M alloy is widely used in crankshaft applications.

Fatigue Test Methodology

A cylindrical fatigue test specimen, shown in Figure 6, was developed, with a stress concentration factor of k_t=1.5 at the root, to provide an economical laboratory scale specimen to evaluate the deep rolling process. Fatigue specimens were machined along the centerlines of the 4140 and NTB steels, and parallel to the centerline at a position 32 mm from the centerline in the C38M material. All fatigue testing was performed in fully reversed (R=-1) flex-beam type fatigue machines at 30 Hz. This procedure is in accordance with resonant frequency type reversed bending fatigue testing of crankshaft journals in industry (1,3,8,9). The baseline material properties were characterized using tension, compression, and fatigue testing.

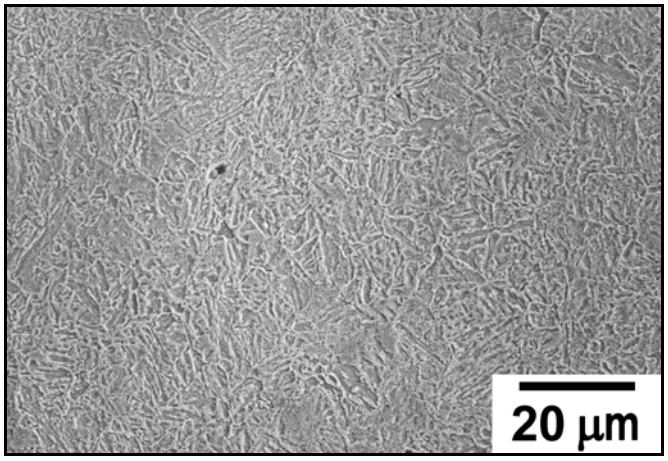

Figure 3. Scanning electron micrograph of 4140 Q&T steel. 2% nital etch, secondary electron image.

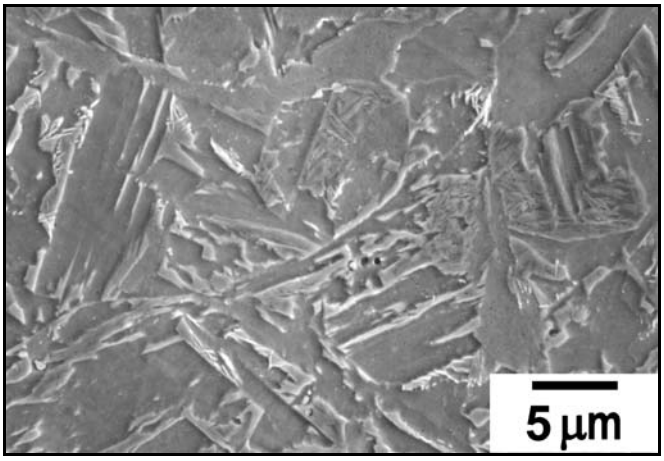

Figure 4. Scanning electron micrograph of as-hot rolled NTB steel. 2% nital and 4% picral etch then gold sputter coated, secondary electron image.

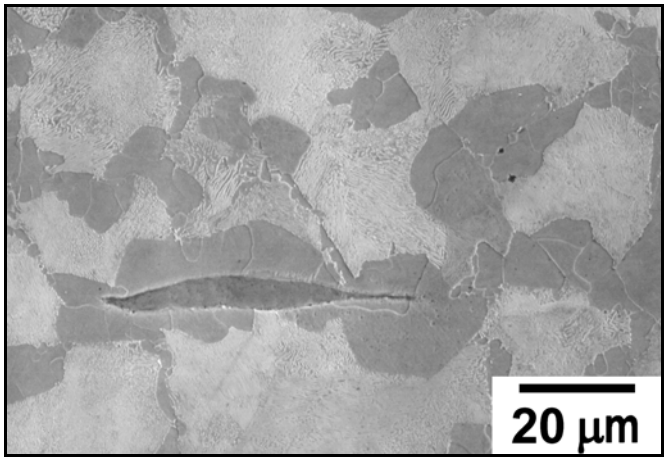

Figure 5. Scanning electron micrograph of C38M steel in the longitudinal direction with MnS particle. 2% nital etch, secondary electron image.

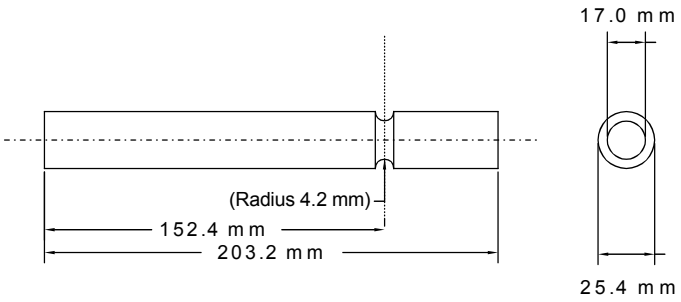

Figure 6. Geometry of the fatigue and deep rolling specimen.

Tension and compression tests were performed at room temperature on a commercial electro-mechanical test system to assess the deformation behavior of the three steels. All tests were performed with an engineering strain rate of $1.6*10^{-3}$ s^{-1}. Tensile tests were performed on round samples with a 40.6 mm long, 6.35 mm diameter, reduced gage length, and strain was measured with a commercial extensometer attached to the gage length. Compression testing was included in this study based on the assumption that the data would better represent the material flow behavior in deep rolling. The compression tests were performed on cylindrical specimens 11.43 mm in height and 7.62 mm in diameter, and platen displacement was measured with a commercial extensometer mounted between the platens, at a location off-center of the loading axis. Due to the loacation of the extensometer, slight errors in elastic deformation were observed. These were accounted for by adjusting all data sets (tension and compression) to the same typical elastic modulus for steel. Both specimen types were machined from the centerline of respective fatigue specimens.

Fatigue testing of the baseline materials incorporated three specimens per stress amplitude with a 68.9 MPa step size between imposed stress amplitudes. From the fatigue data, the endurance limit was defined as the highest stress amplitude where three specimens achieved a run-out of 10^7 cycles. When run-out was achieved the stress amplitude was increased 34.5 MPa and three more specimens were tested.

The effects of deep rolling on the fatigue behavior of the three steels were assessed in two steps. First, data were obtained to optimize the rolling process through assessment of the effects of rolling load on the fatigue behavior, analogous to the results discussed in Figure 1. Samples of each steel were deep rolled with a 108 mm diameter roller having a 3.9 mm radius designed to match the sample notch radius. Multiple samples of each steel were deep rolled with 33 over-rollings. The number of over-rollings was held constant and arbitrarily selected to be in the mid-range of values commonly used in industry.

For the optimization study, the rolling force was varied between 3 kN and 22.5 kN. For each steel a fatigue stress amplitude was selected and held constant based on a consideration of the anticipated endurance limit from previous literature (6,7) and preliminary data at high stress amplitudes that exhibited minimal response to deep rolling, an observation attributed to excessive plastic flow upon cyclic bending. The stress amplitudes selected for the analysis were 572 MPa for the 4140 steel, 552 MPa for the NTB steel, and 524 MPa for the C38M steel. The number of cycles to failure was measured at the selected stress amplitude for each rolling load. Once the rolling load corresponding to optimal fatigue performance was established for each steel, additional specimens were processed at the specified rolling loads. Complete S-N curves were obtained for these deep rolled samples and the results were compared with the baseline fatigue behavior for the unrolled condition.

RESULTS

BASELINE PROPERTIES

Standard mechanical properties of the as-received material, i.e. 0.2 percent offset yield strength, ultimate tensile strength, and total elongation in a 25.4 mm gage length, are summarized in Table 2. The data reveal that the materials chosen for this study exhibit significant differences in yield strength (552 to 848 MPa) with much smaller differences in tensile strength (835 to 946 MPa). Figure 7 shows the true stress versus true strain behavior of the three materials in both tension and compression, where the tensile data are plotted up to the point of instability (i.e. the onset of necking). The results show nearly identical stress-strain behavior in compression and tension testing. Differences in the strain hardening behaviors of the three steels at low strain (i.e. $\varepsilon<0.02$) are amplified in the Jaoul-Crussard plot shown in Figure 8 (10). In a Jaoul-Crussard plot, the true strain-hardening rate is plotted versus plastic strain on a log-log scale. The strain-hardening rate data presented in Figure 8 were obtained through an averaged, linear approximation, in 10^{-4} strain increments, of the data presented in Figure 7. At low strains ($\varepsilon<0.02$), it is evident that the 4140 steel has the lowest strain-hardening rate, the C38M steel has approximately double the strain-hardening rate of 4140, and the NTB steel has approximately triple the strain-hardening rate of 4140 as shown both in Figure 7 and Figure 8. All steels exhibit similar strain hardening behavior at high strains.

Three baseline fatigue tests were run at each imposed stress level and the results are presented in Figures 9 to 11 as standard S-N plots. In each figure a number in parentheses next to a data point indicates multiple tests at the specified condition. The nominal stress amplitudes were calculated based upon a smooth sample of equivalent diameter to that of the reduced diameter at the notch (17.0 mm). This procedure ignores the effect of the stress concentration and provides a means of comparing materials. Excellent reproducibility was obtained at all stress levels as illustrated in Figures 9 to Figure 11. The 4140 steel

demonstrated a nominal endurance limit of 310 MPa (45 ksi) as shown in Figure 9. The NTB material had a nominal endurance limit of 276 MPa (40 ksi), as shown in Figure 10. The C38M material had a nominal endurance limit of 241 MPa (35 ksi), as shown in Figure 11. To further compare measured endurance limits, the stress concentration factor adjusted endurance limits (i.e. k_t*S_f, where k_t=1.5) were calculated for each steel and the results are summarized in Table 3. Also included in Table 3 are calculated fatigue ratios, i.e. the ratio of the adjusted endurance limit to the tensile strength (k_t*S_f/UTS). The fatigue ratios for all three steels are close to 0.5, a commonly accepted approximation for hardened steels (11). This comparison indicates that the measured fatigue properties of the baseline materials are reasonable.

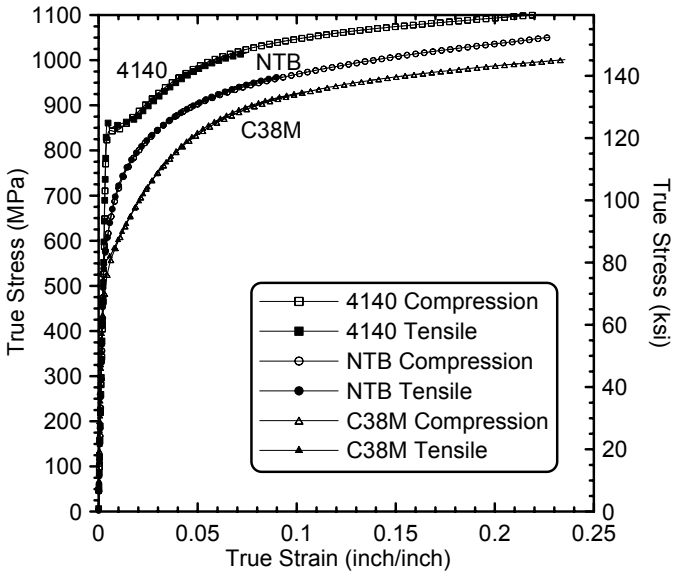

Figure 7. Tension and compression true stress versus true strain relations for the 4140, NTB, and C38M steels. All tests performed at room temperature at an engineering strain rate ($\dot{e}$) of $1.6*10^{-3}$ s^{-1}.

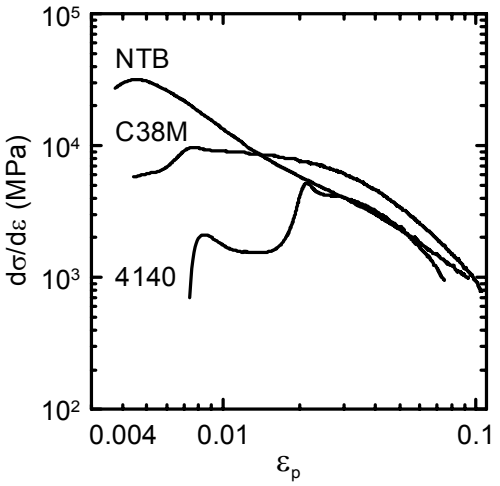

Figure 8. Jaoul-Crussard plot of $d\sigma/d\varepsilon$ versus ε_p for the 4140, NTB, and C38M steels. Plot illustrates amplifies differences in strain-hardening rates between materials at low strains.

TABLE 2. Steel Tensile Property Data

Steel	Eng. 0.2% Yield Stress (MPa)	UTS (MPa)	% Strain to Failure (25.4 mm gage)
4140	848	946	21
NTB	579	881	24
C38M	552	835	20

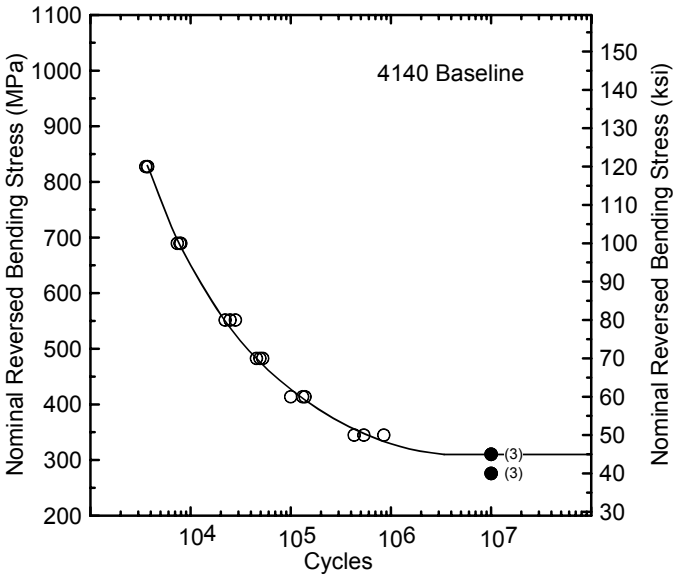

Figure 9. Nominal reversed bending stress versus number of cycles to failure at stress for 4140 steel in the as received condition. Number in parentheses indicate multiple data points.

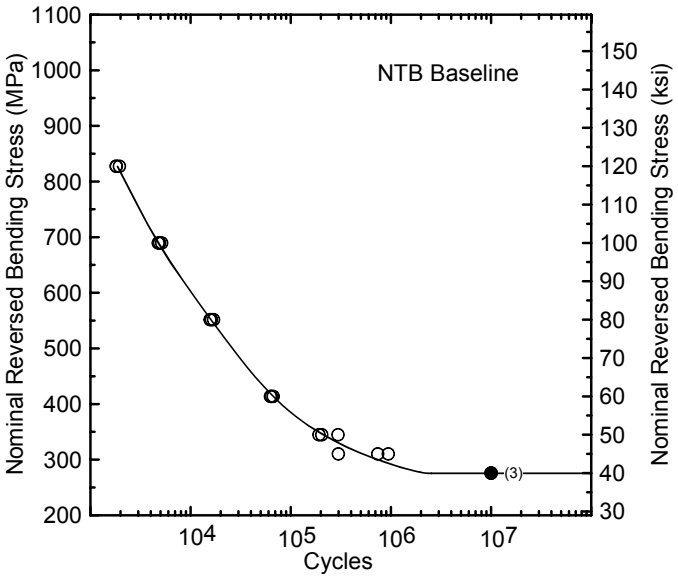

Figure 10. Nominal reversed bending stress versus number of cycles to failure at stress for NTB steel in the as-received condition.

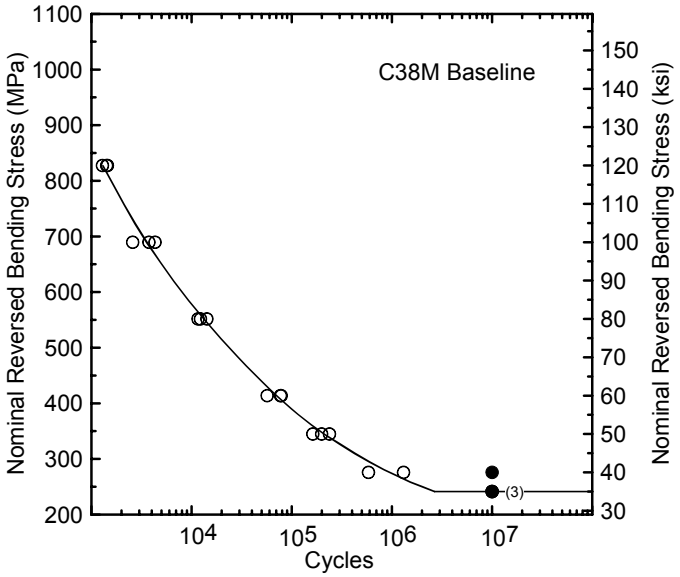

Figure 11. Nominal reversed bending stress versus number of cycles to failure at stress for C38M material in the as-received condition.

TABLE 3. Baseline Fatigue Property Data for Materials Used in this Study

Steel	Nominal Endurance Limit (MPa) $S_{f\text{-}BL}$	Adjusted Endurance Limit (MPa) $S_{f\text{-}BL}*k_t$	Fatigue Ratio $k_t*S_{f\text{-}BL}/UTS$
4140	310	465	0.49
NTB	276	414	0.47
C38M	241	362	0.43

DEEP ROLLED PROPERTIES

Optimization of Rolling Load

Figure 12 shows the fatigue life (cycles to failure) versus applied load in deep rolling. Data for each material were obtained at a constant imposed stress amplitude (values indicated in figure). A trend line was drawn for each steel to represent the average behavior of the data shown in Figure 12. With an increase in rolling force, the fatigue performance improves over the baseline condition. This improvement continues until a maximum performance level is achieved. Consistent with previous studies (4-7), further increases in rolling load degrade the fatigue performance. It is evident that the three materials, which demonstrated similar fatigue behavior in the baseline condition, behave quite differently in the deep rolled condition.

The optimal rolling load was defined as the lowest rolling load that exhibited fatigue life distribution that encompassed the highest average fatigue lives achieved (i.e. the onset of the peak or plateau of the curve). For example, in Figure 12, the C38M material at 10.5 kN rolling force exhibited a fatigue life distribution that achieved equivalent performance to specimens processed at higher rolling forces. The 4140 alloy achieved peak performance at a rolling load of 17.5 kN, the NTB alloy achieved peak performance at a rolling load of 15 kN, and the C38M alloy achieved the peak performance at a rolling load of 10.5 kN. Presumably the lower yield stress levels in the NTB and C38M materials allow the surface to deform at reduced rolling loads while the higher yield stress 4140 alloy exhibits very little response to the lower rolling loads. Once a high enough force was applied to overcome the yield stress in the 4140, the fatigue performance improved substantially with small increases in rolling force. The effects of exceeding the optimal rolling load were apparent in the three materials as an increase in the variance in fatigue life and a decrease in the average performance.

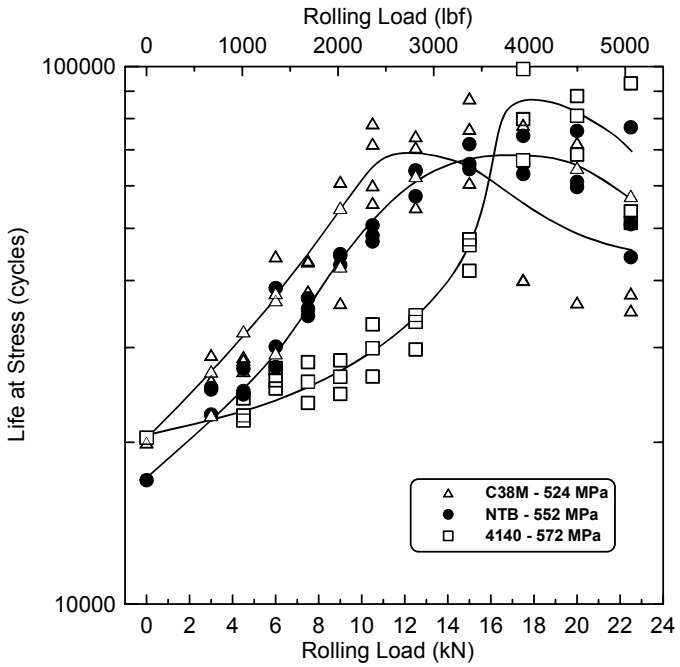

Figure 12. Measured fatigue life at a constant stress versus applied rolling load in deep rolling. The nominal reversed bending stress for each steel is shown in the legend.

Deep Rolled at Optimized Load

Specimens of each material were deep rolled at the optimized condition as described above and were subsequently tested to generate standard S-N type data over a range of applied stress amplitudes. The fatigue test methodology was the same as outlined above with the exception that the imposed stresses were based on the data shown in Figure 12, with data from Figure 12 included in the following S-N diagrams. At the higher stress levels, only a single specimen was tested due to the limited number of specimens and the high degree of reproducibility observed for the high stress tests.

A comparison of the deep rolled S-N data and the baseline S-N data are shown in Figures 13-15. The 4140 steel, deep rolled at 17.5 kN, demonstrated a nominal endurance limit of 469 MPa (68 ksi), the S-N data are shown in Figure 13. The NTB, deep rolled at 15 kN, demonstrated a nominal endurance limit of 448 MPa (65 ksi), the S-N data are shown in Figure 14. The C38M, deep rolled at 10.5 kN, demonstrated a nominal endurance limit of 386 MPa (56 ksi), the S-N data are shown in Figure 15. The deep rolled fatigue data are listed Table 4, which includes nominal endurance limit, adjusted endurance limit, and fatigue ratio.

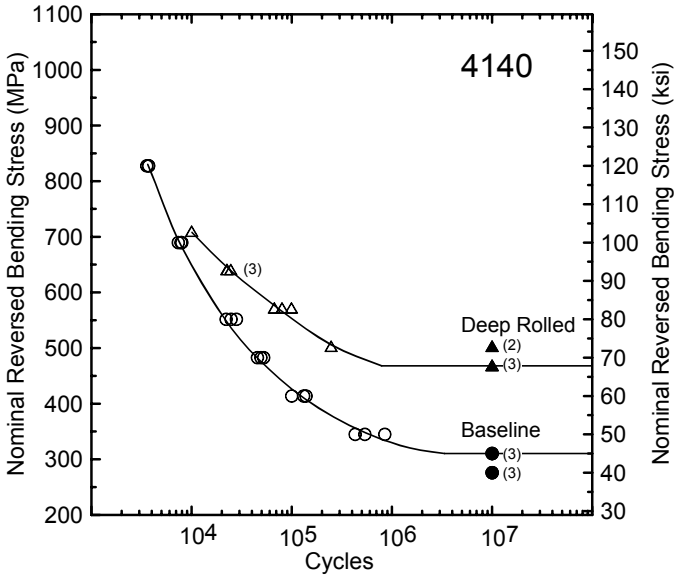

Figure 13. Nominal reversed bending stress versus number of cycles till failure at stress for 4140 material in the optimized, deep rolled condition with the baseline condition presented for comparison. Number in parentheses indicates multiple points.

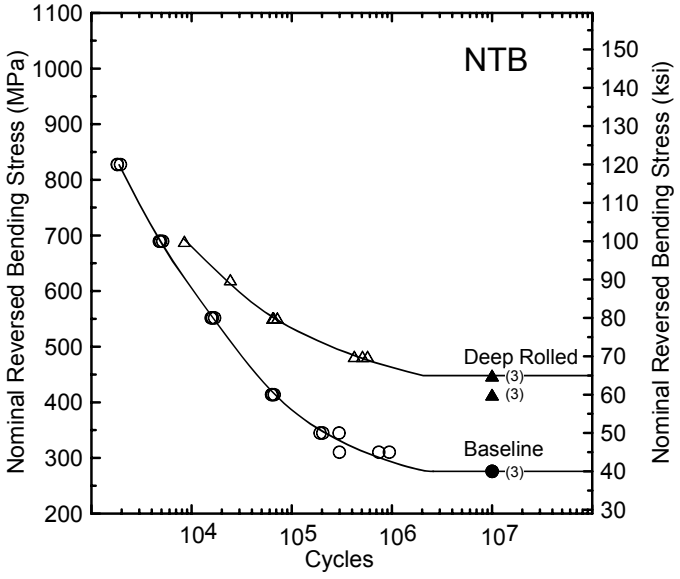

Figure 14. Nominal reversed bending stress versus number of cycles till failure at stress for NTB material in the optimized, deep rolled condition with the baseline condition presented for comparison.

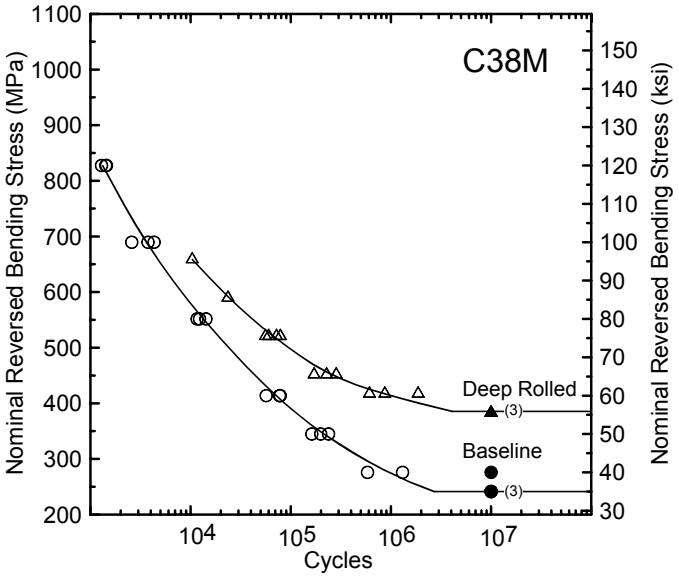

Figure 15. Nominal reversed bending stress versus number of cycles till failure at stress for C38M material in the optimized, deep rolled condition with the baseline condition presented for comparison.

TABLE 4. Deep Rolled Fatigue Property Data for Materials Used in this Study

Steel	Nominal Endurance Limit (MPa) $S_{f\text{-}DR}$	Adjusted Endurance Limit (MPa) $S_{f\text{-}DR}*k_t$	Fatigue Ratio $k_t*S_{f\text{-}DR}/UTS$
4140	469	704	0.74
NTB	448	672	0.76
C38M	386	579	0.69

Table 5 lists the improvements in fatigue properties of the deep rolled condition over the baseline condition. All three materials exhibited a significant increase (>50%) in endurance limit as a result of the deep rolling process. However, while the 4140 alloy exhibited the highest endurance limit, it exhibited the least percentage increase of the three steels. In terms of both magnitude and percentage increase, the NTB alloy demonstrated the highest overall improvement in endurance limit. The C38M was very near the NTB in percentage improvement, but had the lowest endurance limit. The differences between the steels are quite small (in terms of relative improvements from deep rolling) considering the uncertainty in the measured endurance limits.

Further characterization of the optimized deep rolled condition included microhardness profiles that were measured on cross sections at the root of the notch and the data are shown in Figure 16. The 4140 steel with the lowest strain hardening rate of the three alloys, exhibited very little change in hardness versus depth. In contrast, both the NTB and C38M steels had similar microhardness profiles with hardness peaks at approximately 0.3 mm below the surface. In comparison

TABLE 5. Fatigue Improvements of the Deep Rolled versus Baseline Conditions

Steel	Nominal Endurance Limit Change (MPa) ΔS_f	Adjusted Endurance Limit Change (MPa) $\Delta S_f * k_t$	Percent Increase $100\% * \Delta S_f / S_{f\text{-}BL}$
4140	159	239	51
NTB	172	258	62
C38M	145	218	60

to the bulk material measured below 1.5 mm below the surface, the peaks indicated an increase in hardness of approixately 15 HV for the 4140 steel, 60 HV for the NTB, and 50 HV for the C38M. The hardness profiles are consistent with the strain hardening behavior of the three steels (Figures 7 and 8) and the non-uniform strain in the surface due to deep rolling.

It is believed that the variations in hardness profiles between the steels may also reflect different strain gradients in the non-uniform deformation zone due to deep rolling. The non-uniform strains in the deformation zone would then result in correspondingly different residual stress fields between the three steels. This latter point will be considered in a future publication (12).

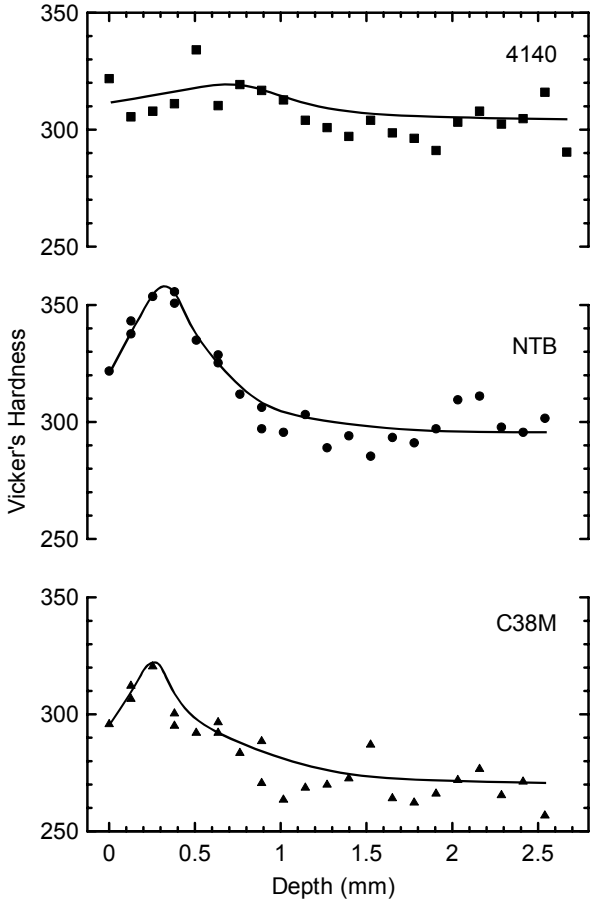

Figure 16. Vicker's Hardness versus depth at the minimum diameter for the three materials tested.

FRACTOGRAPHY

The fracture characteristics of selected fatigue samples were analyzed using standard light fractography techniques. Figures 17 (a)-(d) show the characteristic fracture surfaces from selected test conditions for the NTB steel. The fatigue crack surfaces are characteristic of reversed bending with crack nuclei at the top and bottom of the sample.

Figure 17 (a) shows a baseline specimen tested at low stress amplitude resulting in a life of approximately 10^6 cycles. The sample shows a smooth, stable fatigue crack growth zone characteristic of the high cycle fatigue failure, and a final overload region shifted with respect to the original neutral axis position. The asymmetry reflects the domination of a single crack at low stress until increasing stresses later in the test drive crack initiation on the bottom of the sample. Figure 17 (b) shows a baseline specimen tested at high stress amplitude, resulting in short life. Fatigue cracks nucleated at multiple positions on both top and bottom surfaces, under high stress conditions as evidenced by multiple ratchet marks. Symmetric nucleation and steady crack growth result in a final overload region in the center of the fracture cross section.

Figure 17 (c) shows a NTB specimen deep rolled at the optimal rolling load of 15 kN and tested at 482 MPa, which achieved a life of 570,295 cycles. The fracture surface shows a highly self polished region (outside of the dashed white lines) with multiple ratchet marks that follows the radius from top center to either side. The fracture surface inside of this zone is very similar to the fracture surface in Figure 17 (a). The asymmetry reflects the domination of a single crack propagating through the outer zone resulting in the off-axis final overload region. Figure 17 (d) shows a specimen deep rolled at 15 kN and tested at 689 MPa, which achieved a life of 8467 cycles. The fatigue crack initiated at multiple locations on both the top and bottom sides with large polished regions dominating the top and bottom. The final overload region is centralized as in Figure 17 (b), due to the high stress amplitude and equivalent fatigue crack nucleation and propagation from either surface.

DISCUSSION

The results presented above illustrate systematic interactions between the deformation behavior of the three steels and their subsequent response to deep rolling. Deep rolling provided a substantial increase in the fatigue performance in all three steels as shown in Figures 13-15, increasing the fatigue ratio range from 0.43-0.49 to 0.69-0.74. In previous deep rolling research (1,12) improvements in fatigue performance were attributed to the development of favorable compressive residual stress profiles, an increase in the surface yield strength, and a decrease in surface roughness. In addition to the observed improvement in fatigue performance, deep rolling altered the fatigue fracture surface appearance as shown in Figures 17 (a)

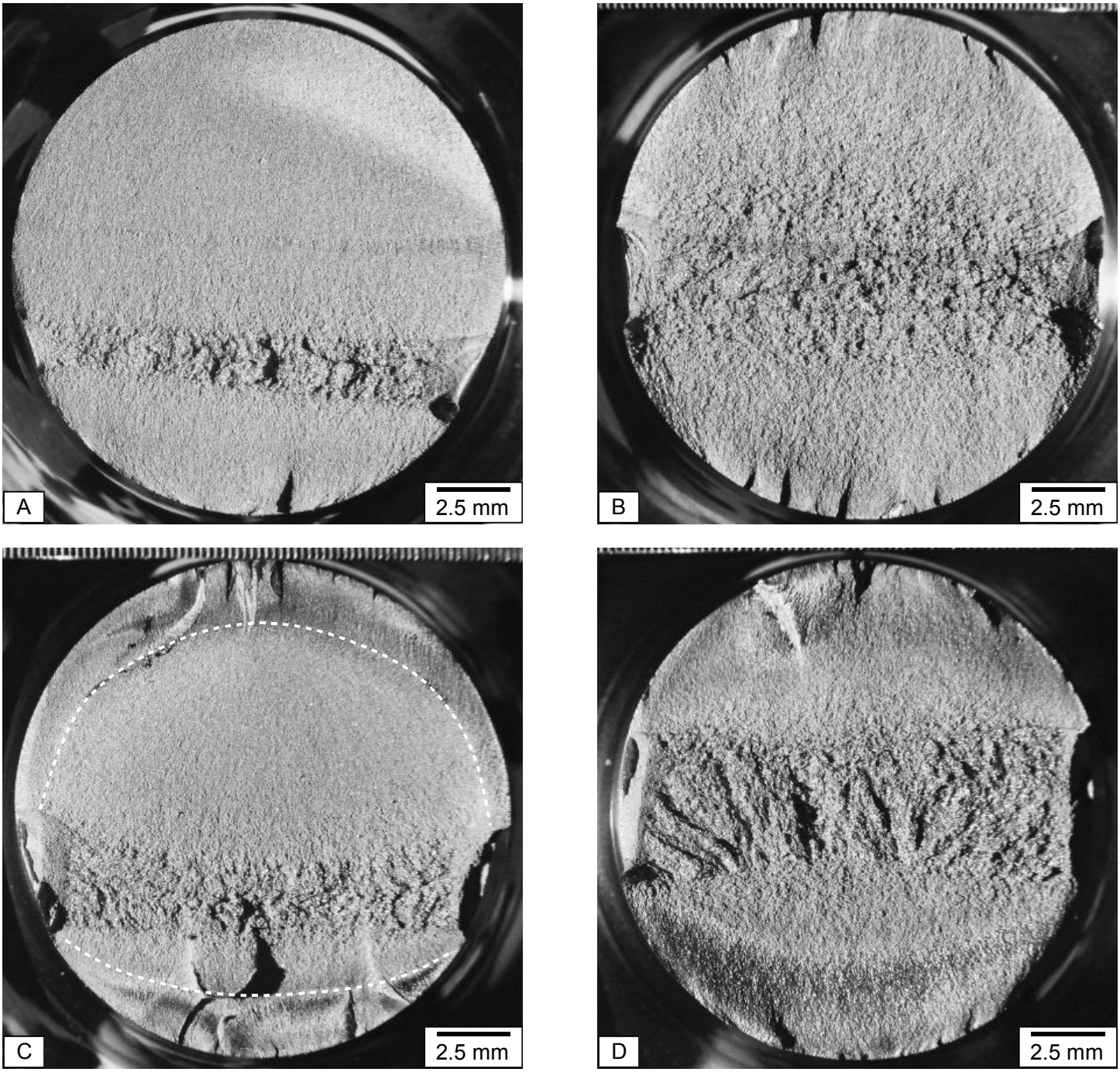

Figure 17. Fractographs of NTB fatigue specimens illustrating the differences in fracture behaviors observed. (a) Baseline, 310 MPa stress amplitude, 940,830 cycles. (b) Baseline, 689 MPa stress amplitude, 4,949 cycles. (c) 15.0 kN rolling load, 482 MPa stress amplitude, 570,295 cycles. (d) 15.0 kN rolling load, 689 MPa stress amplitude, 8,467 cycles.

to 17 (d) and introduced material-dependent hardness gradients as shown in Figure 16. The fracture surfaces show that fatigue crack nucleation and growth in the deep rolled material is associated with an increase in the number of fatigue crack nuclei and extensive surface polishing due to contact between mating fracture surfaces during fatigue. The surface polishing may reflect additional numbers of surface contacts due to an increase in fatigue life or the effects a residual stress profile associated with the non-uniform strain field that was introduced at the notch root and led to the hardness profiles. The presence of a peak in hardness at a location slightly below the surface should also provide a region of strain-hardened material with an increase in fatigue resistance.

It has been shown in Figures 7 and 8 that the three steels, representing three microstructural classes, exhibit vastly different strength levels and strain hardening rates at low strain levels (<0.02). For the optimized condition, the deep rolling process does not significantly change the local geometry, and thus, it is

anticipated that the local strains in the deformation zone below the roller are low. Correspondingly, the type of data shown in Figures 7 and 8 would describe the material flow behavior in the deformation zone and are extremely relevant to assessing potential material response in deep rolling. Future modeling and experimental studies to quantify the local strain gradient and correlate the interrelationships between strain hardening behavior and strain in steels of interest for automotive applications is required to fully clarify these points.

In this study the importance of the strain hardening behavior at low strains is illustrated in the optimization curves shown in Figure 12 and the microhardness profiles in Figure 16. In both figures, the two steels with high strain hardening rates below a strain of 0.02 exhibited similar behavior, i.e. peaks in hardness just below the surface and a rapid increase in fatigue resistance with an increase in rolling load. In contrast the 4140 steel with a higher yield stress, but lower strain hardening rates at low strain, required higher rolling loads to produce measurable increases in fatigue performance and resulted in a hardness profile without the dominant hardness peak illustrated by the other two steels. These results suggest that in addition to correlating standard material properties, e.g. UTS, to the performance of deep rolled parts, careful assessment of additional variables that influence the optimization process must be made to apply deep to efficiently apply deep rolling to future automotive steel grades.

CONCLUSIONS

A test methodology to assess deep rolling on large scale laboratory fatigue specimens was successfully developed and implemented. Fully reversed (R=-1) bending provided excellent reproducibility in fatigue data in both the baseline and deep rolled conditions.

Previous process control methods based on ultimate tensile strength data inadequately predict optimized deep rolling process conditions. It was determined that the material deformation behavior and yield stresses dramatically affect the shape of the optimization curve. An opportunity exists to tailor the process control methodology to steels of current interest, and thereby further enhance the potential benefits that deep rolling can provide.

The endurance limits were closely related to the ultimate tensile stresses in the baseline and deep rolled conditions. Deep rolling provided a significant increase in endurance limit in all three materials. The strain hardening behavior of the material influenced the deep rolling response, and perhaps the improvement in fatigue performance associated with the application of deep rolling.

ACKNOWLEDGMENTS

The authors acknowledge the support of the Advanced Steel Processing and Products Research Center, an Industry-University Cooperative research center at the Colorado School of Mines. The authors also acknowledge the Hegenscheidt-MFD Corp. of Sterling Heights, MI, and in particular Mike Hoeppner, for providing the specialized deep rolling for this study.

REFERENCES

1. E. Randlett, “Deep Rolling of Crankshaft,” SME, MF70-262.

2. H. Naumann, “Deep Rolling of Highly Stressed Components,” American Society of Tool and Manufacturing Engineers, MF68-169, 1968.

3. T. Watmough and M.J. Malatesta, “Strengthening of Ductile Iron of Crankshaft Applications,” American Foundrymen’s Society, Inc., 1984, pp. 83-99.

4. G.N.J. Gilbert, K.B. Palmer, “The influence of surface rolling on the fatigue properties of flake graphite and nodular graphite cast irons,” British Cast Iron Research Institute, Journal of Research and Development, vol. 5, no. 392, 1954, pp. 447-464.

5. K. H. Kloos and J. Adelmann, “Effect of Deep Rolling on Fatigue Properties of Cast Irons,” Journal of the Mechanical Behavior of Materials (UK), vol. 2, no. 1-2, 1989, pp. 75-86.

6. K.H. Kloos, B. Fuchsbauer, and J. Adelmann, “Fatigue properties of specimens similar to components deep rolled under optimized conditions,” International Journal of Fatigue, vol. 9, no. 1, 1987, pp. 35-42.

7. K.H. Kloos, E. Broszeit, B. Fuchsbauer, and F. Schmidt, “Optimierung von Schingfestigkeits-eigenschaften beim Oberflachendrücken gekerbter Umlaufbiegeproben unter Berücksichtigung der ProbengröBe*,” Z. Werkstofftech., vol 12, 1981, pp. 359-365.

8. T.C. Chatterley, P. Murrell, “ADI Crankshaft – An Appraisal of Their Production Potential,” Society of Automotive Engineers, Inc., 980686, 1998, pp. 436-453.

9. H. Park, Y.S. Ko, S.C. Jung, “Fatigue life analysis of crankshafts at various surface treatments,” Society of Automotive Engineers, Inc., 01ATT193, 2001.

10. D.K. Matlock, F. Zia-Ebrahimi, G. Krauss, ”Structure, Properties, and Strain Hardening of Dual-Phase Steels,” Deformation, Processing, and Structure, ASM, 1982, pp 47-87.

11. H.O. Fuchs, R.I. Stephens, “Metal Fatigue in Engineering,” John Wiley & Sons, 1980, pp 68-69.

12. M.D. Richards, D.K. Matlock, J.G. Speer, and A.K. De, Unpublished Research, Colorado School of Mines, Golden, Colorado, 2004.